

Reactions of the Small Tin Clusters with Carbon Monoxide: Infrared Spectra and DFT Calculations of the Sn_nCO ($n = 2$–5) and $Sn_2(CO)_2$ Molecules in Solid Argon

Ling Jiang and Qiang Xu*

National Institute of Advanced Industrial Science and Technology (AIST), 1-8-31 Midorigaoka, Ikeda, Osaka 563-8577

Graduate School of Science and Technology, Kobe University, 1-1 Rokkodai, Nada-ku, Kobe 657-8501

Received November 9, 2005; E-mail: q.xu@aist.go.jp

Laser-ablated Sn atoms have been co-deposited with CO molecules in solid argon to produce tin carbonyls. In addition to the previously reported $Sn(CO)_n$ ($n = 1$ and 2) molecules, small tin cluster carbonyls Sn_nCO ($n = 2$–5) and $Sn_2(CO)_2$ are formed on sample annealing, and are characterized using infrared spectroscopy on the basis of the results of the isotopic substitution, the CO concentration change, and the comparison with theoretical predictions. It is found that Sn_2CO, Sn_3CO, and Sn_5CO are bridge-bonded carbonyl compounds, whereas $Sn_2(CO)_2$ and Sn_4CO are terminal-bonded carbonyl molecules. The $Sn_2(CO)_2$ species observably undergoes photo-induced decomposition to $Sn(CO)_2$. Another interesting finding is that the absorption of Sn_4CO shifts from 1994.0 to 1989.8 cm^{-1} by UV light irradiation, probably due to the change of the electronic state or the matrix effect. The density functional theory calculations have been performed on these molecules and the corresponding small naked tin clusters. Furthermore, energetic analysis for the possible reactions of lead atoms with CO molecules is also given.

Metal clusters and their chemical compounds have attracted considerable attention because they play an important role in such diverse areas as nanomaterials, microelectronics, heterogeneous or homogeneous catalysis, etc.[1–3] Probe molecules (i.e., CO, H_2, H_2O, NO, NH_3, etc.) are usually used to gain insight into their chemisorption characteristics and catalytic activity. Reliable experimental data for neutral and charged clusters can be obtained, such as ionization potentials (IP), electron affinities (EA), magnetic moments, photoelectron spectra, infrared absorption spectra, polarizabilities, optical properties, and ligand adsorption capacities.[3–6] However, it is difficult to directly determine the structure of a metal cluster due to the fact that clusters are often produced in gas-phase beams and are too small (3–50 atoms) for applying diffraction techniques.[3–6] Fortunately, recent advances in methodology based on the technologies of pseudopotential and plane-wave basis sets and high-speed computers have now made it possible to obtain quantitative information on the cluster's structures as well as IP, EA, etc.[1,5,7]

A variety of experimental and theoretical studies on group 14 clusters can be found in the literature.[8–15] The gas-phase electronic spectra of Sn_2 and Pb_2 have been obtained by combining pulsed laser vaporization with laser-induced fluorescence.[8,9] The vibrational frequency of Sn_2 has been reported to be 188 cm^{-1} in the X (O_g^+) ground state in solid argon.[8–10] There have been a few experimental studies on charged lead clusters.[15] The photodetachment spectra of Sn_2^- and Pb_2^- clusters and mixed dimers have been studied and the results have been found to be in very good agreement with the previous theoretical calculations on Sn_2^- and Pb_2^-.[16] Moreover, the ground states of Ge_4, Sn_4, and Pb_4 have been calculated to be ^1A_g states with equilibrium geometries of a rhombus similar to Si_4.[13]

The technique of laser ablation coupled with matrix isolation has proven to be an efficient method to generate neutral atoms and cations of transition metals and main group elements as well as electrons.[17–33] In addition to a large number of mononuclear metal carbonyls, small metal cluster carbonyls, such as Fe_2CO,[18,19] Co_2CO,[20] B_2CO and $B_2(CO)_2$,[21] Sc_2CO,[22] M_nCO (M = Si, Ge, and Pb; $n = 2$–5),[23a–c] and Au_nCO ($n = 1$–5) and $Au_2(CO)_2$,[23d,e] have recently been synthesized via this combined approach. Meanwhile, theoretical investigations have been carried out for Fe_nCO ($n = 1$–6),[24] Cu_nCO ($n = 2$–13),[25] and Ni_2CO.[26] In contrast with considerable experimental and theoretical studies of the interactions of CO molecules with the transition metal and main group element atoms,[27–32] almost nothing is known about the tin cluster carbonyl. Here, we report the observation of small tin cluster carbonyls, Sn_nCO ($n = 2$–5) and $Sn_2(CO)_2$, generated from the reactions of tin atoms with CO molecules in solid argon and characterized using infrared spectroscopy. The density functional theory (DFT) calculations have been performed to support the experimental assignments of the infrared spectra and provide insight into the structures and bonding of the product molecules.

Experimental and Theoretical Procedures

The experiment for laser ablation and matrix isolation infrared spectroscopy is similar to those previously reported.[23b,33] Briefly, the Nd:YAG laser fundamental (1064 nm, 10 Hz repetition rate with 10 ns pulse width) was focused on the rotating tin target. The laser-ablated tin atoms were co-deposited with CO in excess argon onto a CsI window cooled normally to 7 K by means of a closed-cycle helium refrigerator. Typically, 3–15 mJ $pulse^{-1}$ laser power was used. Carbon monoxide (99.95% CO), $^{13}C^{16}O$ (99%,

Published on the web June 6, 2006; doi:10.1246/bcsj.79.857

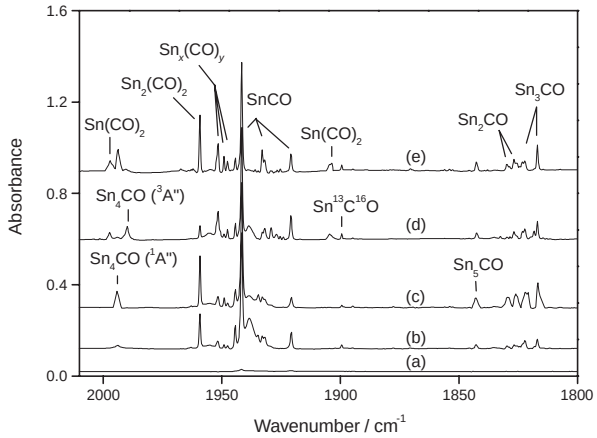

Fig. 1. Infrared spectra in the 2010–1800 cm^{-1} region from co-deposition of laser-ablated Sn atoms with 0.025% CO in Ar. (a) One hour sample deposition at 7 K, (b) after annealing to 30 K, (c) after annealing to 34 K, (d) after 15 min broad-band irradiation, and (e) after annealing to 38 K.

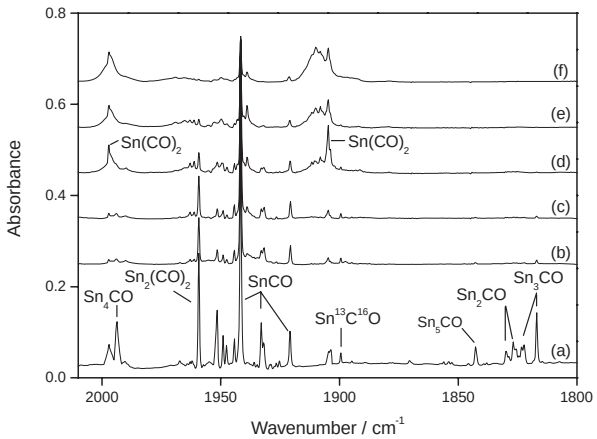

Fig. 2. Infrared spectra in the 2010–1800 cm^{-1} region from co-deposition of laser-ablated Sn atoms with different CO concentration after UV light irradiation and annealing to 38 K in Ar. (a) 0.025% CO, (b) 0.05% CO, (c) 0.1% CO, (d) 0.5% CO, (e) 1.5% CO, and (f) 3.0% CO.

^{18}O <1%), and $^{12}C^{18}O$ (99%) were used to prepare the CO/Ar mixtures. In general, matrix samples were deposited for one to two hours with a typical rate of 2–4 mmol per hour. After sample deposition, IR spectra were recorded on a BIO-RAD FTS-6000e spectrometer at 0.5 cm^{-1} resolution using a liquid nitrogen cooled HgCdTe (MCT) detector for the spectral range of 5000–400 cm^{-1}. Samples were annealed at different temperatures and subjected to broad-band irradiation ($\lambda > 250$ nm) using a high-pressure mercury arc lamp (Ushio, 100 W).

Quantum chemical calculations were performed to predict the structures and vibrational frequencies of the observed reaction products using the Gaussian 03 program.[34] The Becke three parameter hybrid functional with the Lee–Yang–Parr correlation corrections (B3LYP) was used.[35,36] The 6-311+G(d) basis sets were used for C and O atoms,[37] and the Los Alamos ECP plus DZ (LANL2DZ) for Sn atoms.[38] Geometries were fully optimized and vibrational frequencies were calculated with analytical second derivatives. The previous investigations have shown that the use of hybrid B3LYP along with ECP can provide reliable information

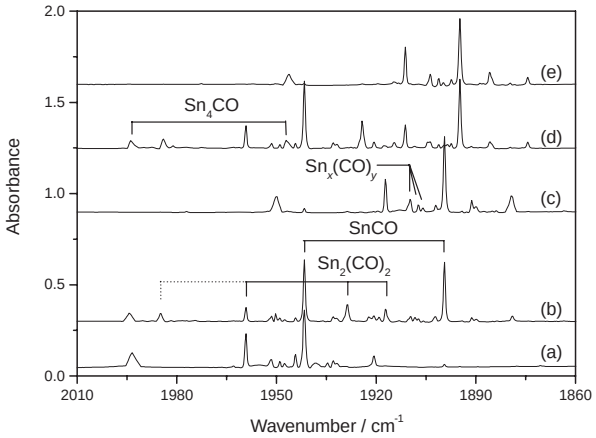

Fig. 3. Infrared spectra in the 2010–1860 cm^{-1} region for laser-ablated Sn atoms co-deposited with isotopic CO in Ar after annealing to 34 K. (a) 0.025% $^{12}C^{16}O$, (b) 0.02% $^{12}C^{16}O$ + 0.02% $^{13}C^{16}O$, (c) 0.025% $^{13}C^{16}O$, (d) 0.02% $^{12}C^{16}O$ + 0.02% $^{12}C^{18}O$, and (e) 0.025% $^{12}C^{18}O$.

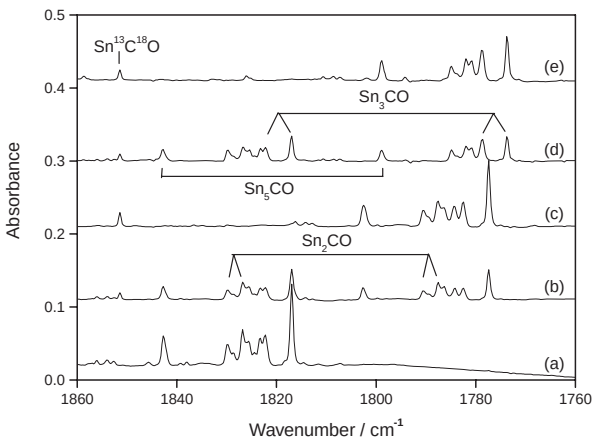

Fig. 4. Infrared spectra in the 1860–1760 cm^{-1} region for laser-ablated Sn atoms co-deposited with isotopic CO in Ar after annealing to 34 K. (a) 0.025% $^{12}C^{16}O$, (b) 0.02% $^{12}C^{16}O$ + 0.02% $^{13}C^{16}O$, (c) 0.025% $^{13}C^{16}O$, (d) 0.02% $^{12}C^{16}O$ + 0.02% $^{12}C^{18}O$, and (e) 0.025% $^{12}C^{18}O$.

for tin carbonyls, such as infrared frequencies, relative absorption intensities, and isotopic shifts.[29b]

Results and Discussion

Experiments have been done with carbon monoxide concentrations ranging from 0.025 to 3.0% in argon. Typical infrared spectra for the reactions of laser-ablated tin atoms with CO molecules in excess argon in the selected regions are shown in Figs. 1–4, and the product absorptions are listed in Table 1. The stepwise annealing and photolysis behavior of the product absorptions is also shown in the figures and will be discussed below. In addition, doping with CCl_4 has no effect on these bands (not shown here), suggesting that the products are neutral.

Quantum chemical calculations have been performed on all the possible isomers of the potential product molecules. The most stable structures optimized by hybrid B3LYP calculations for tin carbonyls are displayed in Fig. 5. The ground

Table 1. Infrared Absorptions (cm^{-1}) Observed after Co-Deposition of Laser-Ablated Sn Atoms with CO in Excess Argon at 7 K

$^{12}C^{16}O$	$^{13}C^{16}O$	$^{12}C^{18}O$	$^{12}C^{16}O + {}^{13}C^{16}O$	$^{12}C^{16}O + {}^{12}C^{18}O$	R(12/13)	R(16/18)	Assignment
1997.1	1952.8		1997.2, 1979.8, 1952.8		1.0227		$Sn(CO)_2$ sym
1994.0	1950.3	1946.5	1994.0, 1950.3	1993.9, 1946.7	1.0224	1.0244	Sn_4CO
			1985.0	1984.0			$Sn_2(CO)_2$ sym
1959.2	1917.2	1911.2	1959.2, 1928.7, 1917.1	1959.2, 1924.2, 1911.2	1.0219	1.0251	$Sn_2(CO)_2$ asym
1951.7	1909.7	1903.7			1.0220	1.0252	$Sn_x(CO)_y$
1949.0	1907.3	1901.2			1.0219	1.0251	$Sn_x(CO)_y$
1947.6	1905.9	1898.8			1.0219	1.0257	$Sn_x(CO)_y$
1944.2	1902.0	1897.4	1944.3, 1902.2	1944.3, 1897.4	1.0222	1.0247	SnCO site
1941.6	1899.4	1894.8	1941.6, 1899.4	1941.6, 1894.8	1.0222	1.0247	SnCO
1938.5	1896.3	1891.7	1938.5, 1896.3	1938.5, 1891.7	1.0223	1.0247	SnCO site
1932.9	1891.2	1885.8	1932.9, 1891.2	1932.6, 1885.8	1.0221	1.0250	SnCO site
1920.8	1879.0	1874.4	1920.7, 1879.0	1920.6, 1874.4	1.0223	1.0248	SnCO site
1904.7	1863.5		1904.7, 1879.2, 1863.5		1.0222		$Sn(CO)_2$ asym
1842.7	1802.5	1798.9	1842.7, 1802.6	1842.8, 1798.9	1.0223	1.0244	Sn_5CO
1829.9	1790.5	1784.9	1829.8, 1790.5	1829.8, 1784.9	1.0220	1.0252	Sn_2CO site
1826.8	1787.6	1782.0	1826.8, 1787.5	1826.7, 1781.9	1.0219	1.0251	Sn_2CO
1822.3	1782.5	1778.8	1822.3, 1782.5	1822.2, 1778.7	1.0223	1.0245	Sn_3CO site
1817.0	1777.4	1773.7	1817.0, 1777.4	1817.0, 1773.7	1.0223	1.0244	Sn_3CO

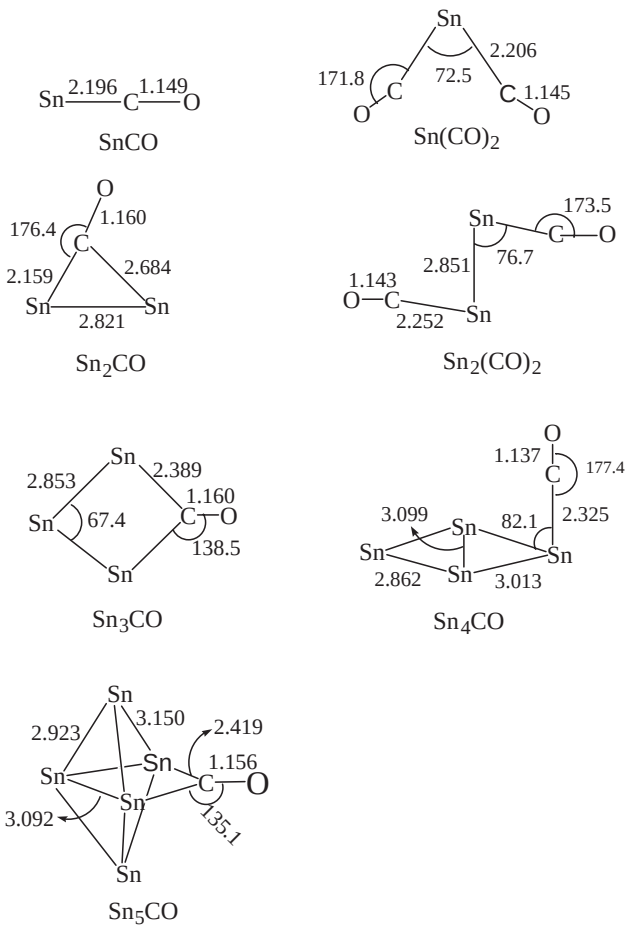

Fig. 5. Optimized structures of the reaction products (bond length in Å, bond angle in degree).

states, point groups, vibrational frequencies, and intensities are listed in Table 2.

$Sn_2(CO)_2$ Molecule. The absorption at 1941.6 cm^{-1} with trapping sites at 1944.2, 1938.5, 1932.9, and 1920.8 cm^{-1} (Table 1 and Fig. 1) is due to the C–O stretching vibration of the SnCO molecule; this is consistent with the previous reports of 1921.0 and 1941.1 cm^{-1} absorptions in Kr[29a] and Ar,[29b] respectively. As reported previously,[29b] the 1997.1 and 1904.7 cm^{-1} bands (Table 1 and Fig. 1) are due to the symmetric and antisymmetric C–O stretching modes of the bent $Sn(CO)_2$ molecule, respectively.

The absorption at 1959.2 cm^{-1} appears on sample annealing, decreases on broad-band irradiation, and recovers on further annealing, as shown in Fig. 1. The 1959.2 cm^{-1} band shifts to 1917.2 cm^{-1} with $^{13}C^{16}O$, and to 1911.2 cm^{-1} with $^{12}C^{18}O$ (Table 1 and Fig. 3). In the mixed $^{12}C^{16}O + {}^{13}C^{16}O$ experiment (Fig. 3), a triplet at 1959.2, 1928.7, and 1917.1 cm^{-1} together with a weak associated band at 1985.0 cm^{-1} is observed. A similar isotopic splitting feature is obtained in the mixed $^{12}C^{16}O + {}^{12}C^{18}O$ isotopic spectra (Fig. 3). As can be seen in Fig. 2, the 1959.2 cm^{-1} band sharply increases with lower CO concentration (0.025%) and higher laser power (10 mJ $pulse^{-1}$) (Fig. 2a), whereas the reverse is true for the relative yields of $Sn(CO)_2$ bands. In the 0.025% CO (10 mJ $pulse^{-1}$) experiment, the intensity ratio of the 1959.2 and 1941.6 cm^{-1} bands is 0.186:0.426, while this ratio changes to 0.042:0.369 in the 0.5% CO (3 mJ $pulse^{-1}$) experiment, suggesting that the species with the 1959.2 cm^{-1} absorption involves more Sn atoms than SnCO and $Sn(CO)_2$. Analogous to the $Si_2(CO)_2$[23a] and $Ge_2(CO)_2$ molecules,[23c] this band is assigned to the antisymmetric C–O stretching mode of $Sn_2(CO)_2$. The bands observed at 1985.0 cm^{-1} in the mixed $^{12}C^{16}O + {}^{13}C^{16}O$ experiment and 1984.0 cm^{-1} in the $^{12}C^{16}O + {}^{12}C^{18}O$ experiment are due to the symmetric C–O stretching modes of $Sn_2(^{12}CO)(^{13}CO)$ and $Sn_2(C^{16}O)(C^{18}O)$, respectively.

The assignment is strongly supported by the present DFT calculations, which predict this $Sn_2(CO)_2$ molecule to have C_{2h} symmetry with an ^1A_g ground electronic state (Table 2 and Fig. 5). The antisymmetric C–O stretching frequency is calculated to be 2024.1 cm^{-1}, which requires a 0.968 scale factor. The calculated $^{12}C^{16}O/{}^{13}C^{16}O$ and $^{12}C^{16}O/{}^{12}C^{18}O$ isotopic frequency ratios of 1.0224 and 1.0254 are again in good

Table 2. Ground Electronic State, Point Group, Vibrational Frequencies (cm^{-1}), and Intensities ($km\,mol^{-1}$) of the Reaction Products Calculated at the B3LYP/6-311+G(d)-LANL2DZ Level

Species	Elec State	Point Group	Frequency (Intensity, Mode)
SnCO	$^3\Sigma^-$	$C_{\infty v}$	1986.2 (1127, σ), 277.2 (1, σ), 236.7 (0.2 × 2, π)
$Sn(CO)_2$	$^1A_1$	C_{2v}	2070.0 (625, A_1), 2002.2 (1177, B_2), 423.0 (22, A_1), 325.3 (0, A_2), 99.8 (0.1, B_2), 288.1 (0.1, A_1), 265.1 (6, B_1), 248.7 (5, B_2), 76.2 (1, A_1)
Sn_2CO	$^1A'$	C_s	1917.5 (769, A′), 374.8 (30, A′), 316.6 (6, A″), 307.5 (3, A′), 171.0 (1, A′), 70.2 (1, A′)
$Sn_2(CO)_2$	^1A_g	C_{2h}	2061.9 (0, A_g), 2024.1 (2414, B_u), 381.7 (0, A_g), 342.2 (17, B_u), 327.0 (5, A_u), 255.5 (0, A_g), 253.9 (0, B_g), 222.6 (31, B_u), 161.6 (0, A_g), 68.8 (0, A_g), 53.4 (2, B_u), 43.1 (0.4, A_u)
Sn_3CO	$^1A_1$	C_{2v}	1909.9 (862, A_1), 354.9 (0.2, B_2), 334.4 (0.5, B_1), 228.3 (0.7, A_1), 174.2 (0.8, A_1), 158.4 (0.1, B_2), 129.1 (2, B_2), 128.8 (7, A_1), 53.6 (1, B_1)
Sn_4CO	$^1A'$	C_s	2088.3 (950, A′), 330.4 (23, A′), 263.7 (1, A″), 183.1 (8, A″), 168.9 (2, A′), 146.1 (2, A′), 139.1 (0.5, A″), 107.9 (1, A′), 69.6 (0, A″), 57.2 (2, A′), 40.9 (0.1, A″), 38.0 (0.1, A′)
Sn_5CO	$^1A_1$	C_{2v}	1935.3 (818, A_1), 338.3 (0.4, B_1), 327.5 (0.1, B_2), 220.0 (0.4, A_1), 163.8 (4, B_1), 154.0 (0.2, A_1), 148.3 (0, B_2), 123.8 (2, A_1), 113.5 (0.7, B_2), 112.5 (1, A_1), 93.6 (0, A_2), 90.9 (1, B_1), 74.0 (0, A_1), 42.0 (0.2, B_2), 2.6 (0.1, B_1)

agreement with the experimental observations, 1.0219 and 1.0251, respectively. We also note that the $Sn_2(CO)_2$ species observably undergo photo-induced decomposition to $Sn(CO)_2$, as shown in Fig. 1 and will be discussed in detail later (vide infra).

Sn_nCO (n = 2–5) Molecule. The present infrared spectra also provide evidence for the formation of small tin cluster carbonyls in the excess argon matrices. For instance, new bands at 1826.8, 1817.0, 1994.0, and 1842.7 cm^{-1} are observed on sample annealing. The experiments with low CO concentrations and high laser energies are of particular interest here. The experimental condition of lower CO concentration and higher laser power favors the formation of these bands. Each band has some trapping site absorptions (Table 1 and Fig. 1) and we will focus on the main bands.

The 1826.8, 1817.0, 1994.0, and 1842.7 cm^{-1} absorptions shift to 1787.6, 1777.4, 1950.3, and 1802.5 cm^{-1} with $^{13}C^{16}O$, and to 1782.0, 1773.7, 1946.5, and 1798.5 cm^{-1} with $^{12}C^{18}O$, respectively. In the mixed $^{12}C^{16}O + {}^{13}C^{16}O$ and $^{12}C^{16}O + {}^{12}C^{18}O$, only pure isotopic counterparts are observed. The isotopic ratios ($^{12}C^{16}O/{}^{13}C^{16}O$: 1.0219, 1.0223, 1.0224, and 1.0223; $^{12}C^{16}O/{}^{12}C^{18}O$: 1.0251, 1.0244, 1.0244, and 1.0244, respectively) and the mixed isotopic characteristic (Figs. 3 and 4) indicate that only one CO subunit is involved in each mode.[39] On the basis of their different isotopic frequency shifts and different annealing and photolysis behavior, each of these bands is attributed to one of the tin cluster carbonyls, Sn_nCO with $n \geq 2$. The 1826.8, 1817.0, and 1842.7 cm^{-1} absorptions lie in the region expected for the bridge-bonded C–O stretching vibrations, whereas the 1994.0 cm^{-1} band is due to a terminal-bonded C–O stretching vibration. It is expected that a high Sn/CO ratio favors the formation of higher clusters during annealing, as will be discussed in detail later. Analogous to the previous reported M_nCO (M = Si, Ge, and Pb; n = 2–5),[23a–c] these bands are assigned to the C–O stretching vibrations of small tin cluster Sn_nCO (n = 2–5) carbonyls, respectively, based on the results of the isotopic substitution and the CO concentration change, and the comparison with theoretical predictions (vide infra).

It can be found that the calculated frequencies are in excellent agreement (only 2.3, 1.1, 1.0, and 1.1% higher, respectively) with the experimental values (Tables 1 and 2). As shown in Fig. 5, the optimized results predict that the most stable structures of Sn_2CO, Sn_3CO, Sn_4CO, and Sn_5CO include semi-bridge, bridge, terminal, and bridge-bonded carbonyls, respectively.

The present optimized Sn–Sn distance in the naked Sn_2 cluster is 2.873 Å, in accord with the previous relativistic calculations (2.76 Å).[11] The Sn–Sn stretching of the Sn_2 cluster is IR inactive, whereas the vibrational frequency of Sn_2 was observed at 188 cm^{-1} in a study of emission and laser excitation spectra.[8–10] Sn_2 has the X (O_g^+) ground state.[8] The present DFT calculations predict that Sn_2CO has an asymmetric structure with an $^1A'$ ground state (Table 2 and Fig. 5). There are two inequivalent Sn–C bond lengths in Sn_2CO (i.e., 2.159 and 2.684 Å). For Sn_2CO, the Sn–Sn bond length is 2.821 Å, which is 0.052 Å shorter than that of Sn_2.

The naked Sn_3 cluster has an $^1A_1$ ground state with C_{2v} symmetry, exhibiting an open obtuse angle structure with an apex angle of 85.1°, which is in accordance with the previous studies.[12] The calculated results predict that Sn_3CO has an $^1A_1$ ground state with two equivalent Sn–C bonds (2.389 Å). In Sn_3CO, the apex angle (67.4°) is 17.7 degrees smaller than that of Sn_3 at the same DFT level.

For Sn_4, a planar rhombus arrangement with D_{2h} symmetry in the ^1A_g ground state is the most stable structure, which is in agreement with the previous studies.[13,14] The most stable structure of Sn_4CO is predicted to have an $^1A'$ ground state with a nonplanar geometry of C_s symmetry. The CO molecule is terminally bonded to one of the apex Sn atoms near the

Table 3. Energetics for Possible Reactions of Tin Atoms with CO Calculated at the B3LYP/6-311+G(d)-LANL2DZ Level

Reaction		Reaction energy[a]/kJ mol^{-1}
1	Sn ($^3P_0$) + Sn ($^3P_0$) → Sn_2 (O_g^+)	−195.0
2	Sn_2 (O_g^+) + Sn ($^3P_0$) → Sn_3 ($^1A_1$)	−215.4
3	Sn ($^3P_0$) + Sn_3 ($^1A_1$) → Sn_4 (^1A_g)	−286.5
4	Sn_2 (O_g^+) + Sn_2 (O_g^+) → Sn_4 (^1A_g)	−306.9
5	Sn ($^3P_0$) + Sn_4 (^1A_g) → Sn_5 ($^1A_1'$)	−215.2
6	Sn_2 (O_g^+) + Sn_3 ($^1A_1$) → Sn_5 ($^1A_1'$)	−306.7
7	Sn ($^3P_0$) + CO → SnCO ($^3\Sigma^-$)	−76.6
8	SnCO ($^3\Sigma^-$) + CO → $Sn(CO)_2$ ($^1A_1$)	−26.6
9	Sn_2 (O_g^+) + CO → Sn_2CO ($^1A'$)	−60.8
10	SnCO ($^3\Sigma^-$) + Sn ($^3P_0$) → Sn_2CO ($^1A'$)	−179.2
11	SnCO ($^3\Sigma^-$) + SnCO ($^3\Sigma^-$) → $Sn_2(CO)_2$ (^1A_g)	−157.6
12	$Sn(CO)_2$ ($^1A_1$) + Sn ($^3P_0$) → $Sn_2(CO)_2$ (^1A_g)	−207.7
13	Sn_2CO ($^1A'$) + CO → $Sn_2(CO)_2$ (^1A_g)	−55.0
14	Sn_3 ($^1A_1$) + CO → Sn_3CO ($^1A_1$)	−92.5
15	SnCO ($^3\Sigma^-$) + Sn_2 (O_g^+) → Sn_3CO ($^1A_1$)	−231.2
16	Sn_2CO ($^1A'$) + Sn ($^3P_0$) → Sn_3CO ($^1A_1$)	−247.0
17	Sn_4 (^1A_g) + CO → Sn_4CO ($^1A'$)	−11.8
18	SnCO ($^3\Sigma^-$) + Sn_3 ($^1A_1$) → Sn_4CO ($^1A'$)	−221.7
19	Sn_2CO ($^1A'$) + Sn_2 (O_g^+) → Sn_4CO ($^1A'$)	−257.8
20	Sn_3CO ($^1A_1$) + Sn ($^3P_0$) → Sn_4CO ($^1A'$)	−205.8
21	Sn_5 ($^1A_1'$) + CO → Sn_5CO ($^1A_1$)	−33.4
22	SnCO ($^3\Sigma^-$) + Sn_4 (^1A_g) → Sn_5CO ($^1A_1$)	−172.0
23	Sn_2CO ($^1A'$) + Sn_3 ($^1A_1$) → Sn_5CO ($^1A_1$)	−279.3
24	Sn_3CO ($^1A_1$) + Sn_2 (O_g^+) → Sn_5CO ($^1A_1$)	−247.7
25	Sn_4CO ($^1A'$) + Sn ($^3P_0$) → Sn_5CO ($^1A_1$)	−236.9
26	Sn_4CO ($^1A'$) → Sn_4CO ($^3A''$)	+62.5

a) A negative value of energy denotes that the reaction is exothermic.

rhombus Sn_4 and is nearly perpendicular to the Sn_4 plane. The ∠CSnSn was calculated to be 82.1°.

The naked Sn_5 cluster is predicted to have an $^1A_1'$ ground state with D_{3h} symmetry, in line with the recent molecular dynamics simulation.[14] Similar to Si_5CO[23a] and Ge_5CO,[23b] the most stable Sn_5CO structure has an $^1A_1$ ground state with C_{2v} symmetry, and CO is bridge-bonded with two of the equatorial Sn atoms of Sn_5 (Fig. 5). In contrast, Au_5CO was found to have a $^2B_2$ ground state with C_{2v} symmetry, and CO is bridge-bonded to two Au atoms of Au_5.[23]

In addition, the calculated net charges of Sn_nCO (n = 2–5) are −0.3642, −0.3077, −0.0826, and −0.3244, respectively. Similar to other well characterized carbonyl species, the interaction between Sn_n and CO can be described as Lewis acid–base bonding, in which CO is regarded as a σ donor and π acceptor, and the contribution from the latter is larger than that from the former.

Several other absorptions at 1951.7, 1949.0, and 1947.6 cm^{-1} (Table 1) are favored by higher laser energy and are due to higher polynuclear tin carbonyls; however, the mixed $^{12}C^{16}O$ + $^{13}C^{16}O$ and $^{12}C^{16}O$ + $^{12}C^{18}O$ isotopic structures could not be resolved. These bands are tentatively assigned to the $Sn_x(CO)_y$ molecules.

Reaction Mechanisms. With low CO concentrations and high laser energies, the laser-ablated tin atoms react with CO molecules in the excess argon matrix to produce the small tin cluster carbonyls, Sn_nCO (n = 2–5) and $Sn_2(CO)_2$, in addition to $Sn(CO)_n$ (n = 1 and 2) (Fig. 1).

Under the present experimental conditions, tin atoms are the predominant species produced by laser ablation of the tin target. The Sn_nCO (n = 2–5) species appear upon sample annealing and increase significantly upon further annealing to high temperatures (30–38 K) in experiments with low CO concentrations (See Fig. 1), which indicates that these small tin clusters are mainly formed in solid argon upon annealing but not during the laser ablation process. This means that the higher laser power leads neither to generating more clusters in the gas-phase, nor to significant annealing of the matrix during deposition therefore increasing the yield of the Sn_n species. It seems that a higher laser power accounts for the generation of a higher concentration of Sn in the matrix, corresponding to a higher Sn/CO ratio.

The energetic analysis for possible reactions of tin atoms and small clusters with CO molecules has been performed at the B3LYP/6-311+G(d)-LANL2DZ level. As can be seen in Table 3, all the possible reactions of tin atoms and small clusters with CO are exothermic (−11.8– −279.3 kJ mol^{-1}). This implies that the diffusion during annealing may make a species, e.g., a tin atom or cluster, a CO molecule, or a tin carbonyl intermediate, in the matrix readily react with its nearest neighbor, and consequently, the final product distribution will mainly depend on the Sn/CO ratio; this is in agreement with our observations that low CO concentration and high laser power favor high nuclearity of cluster molecules (Fig. 2). In contrast, at a high CO concentration and low laser power, corresponding to a low Sn/CO ratio, mononuclear tin poly-

carbonyl species are the predominant products.

Interestingly, the absorption of $Sn(CO)_2$ molecules appears after broad-band irradiation at the expense of $Sn_2(CO)_2$, suggesting that the decomposition of $Sn_2(CO)_2$ to $Sn(CO)_2$ requires some activation energy or is endothermic. At the B3LYP/6-311+G(d)-LANL2DZ level, the generation of $Sn(CO)_2$ from a simple addition reaction of SnCO with CO is slightly exothermic ($-26.6\,kJ\,mol^{-1}$), whereas the decomposition of $Sn_2(CO)_2$ to $Sn(CO)_2$ is endothermic ($207.7\,kJ\,mol^{-1}$), which is in good agreement with the present observation. Another interesting finding is that the Sn_4CO molecule shifts from 1994.0 to $1989.8\,cm^{-1}$ after UV light irradiation and recovers upon further annealing (see Figs. 1d and 1e). The DFT calculations predict that the triplet Sn_4CO molecule ($\nu_{C-O} = 2024.3\,cm^{-1}$) lies $62.5\,kJ\,mol^{-1}$ higher than the singlet one ($2088.3\,cm^{-1}$), which could be obtained by broad-band irradiation ($\lambda > 250\,nm$). The red-shift of Sn_4CO infrared absorption by UV light irradiation may be due to the change of the electronic state, whereas the matrix effect could also be responsible for this shift.

Conclusion

Reactions of laser-ablated Sn atoms with CO molecules in solid argon have been studied using matrix-isolation infrared spectroscopy. In addition to the previously reported SnCO and $Sn(CO)_2$ molecules, the small tin cluster carbonyls Sn_nCO ($n = 2$–5), and $Sn_2(CO)_2$ are observed in the present infrared spectra. Based on the results of the isotopic substitution, stepwise annealing, change of CO concentration and laser energy, and the comparison with theoretical predictions, the absorptions at 1826.8, 1817.0, 1994.0, and $1842.7\,cm^{-1}$ have been assigned to Sn_2CO, Sn_3CO, Sn_4CO, and Sn_5CO, respectively. Among the small tin cluster mono-carbonyls, bridging CO is found in Sn_2CO, Sn_3CO, or Sn_5CO, whereas terminal CO is found in Sn_4CO. The $1959.2\,cm^{-1}$ band is due to the antisymmetric C–O stretching mode of $Sn_2(CO)_2$, which undergoes photo-induced decomposition to $Sn(CO)_2$. In addition, the absorption of Sn_4CO shifts from 1994.0 to $1989.8\,cm^{-1}$ by UV light irradiation, which may be due to the change of the electronic state or the matrix effect. The observation of Sn_nCO ($n = 2$–5) and $Sn_2(CO)_2$ is in good agreement with the prediction of density functional theory calculations.

We gratefully acknowledge financial support for this research by a Grant-in-Aid for Scientific Research (B) (Grant No. 17350012) from the Ministry of Education, Culture, Sports, Science and Technology (MEXT) of Japan and by Marubun Research Promotion Foundation. L. J. thanks MEXT of Japan and Kobe University for an Honors Scholarship.

References

1 J. A. Alonso, *Chem. Rev.* **2000**, *100*, 637.

2 A. Kaldor, D. M. Cox, M. R. Zakin, *Adv. Chem. Phys.* **1988**, *70*, 211.

3 P. Braunstein, L. A. Oro, P. R. Raithby, *Metal Clusters in Chemistry*, Wiley-VCH, Weinheim, Germany, **1999**.

4 A. Rosen, *Adv. Quantum Chem.* **1998**, *30*, 235.

5 a) N. Rösch, G. Pacchioni, *Inorg. Chem.* **1990**, *29*, 2901. b) N. Rösch, L. Ackermann, G. Pacchioni, *J. Am. Chem. Soc.* **1992**, *114*, 3549.

6 G. Meloni, R. W. Schmude, J. E. Kingcade, Jr., K. A. Gingerich, Jr., *J. Chem. Phys.* **2000**, *113*, 1852.

7 C. H. Chien, E. Blaisten-Barojas, M. R. Pederson, *Phys. Rev. A* **1998**, *58*, 2196.

8 V. E. Bondybey, J. H. English, *J. Chem. Phys.* **1977**, *67*, 3405.

9 V. E. Bondybey, J. H. English, *J. Chem. Phys.* **1982**, *76*, 2165.

10 M. A. Epting, M. T. Mckenzie, Jr., E. R. Nixon, *J. Chem. Phys.* **1980**, *73*, 134.

11 K. Balasubramanian, K. S. Pitzer, *J. Chem. Phys.* **1983**, *78*, 321.

12 K. Balasubramanian, *J. Chem. Phys.* **1986**, *85*, 3401.

13 D. G. Dai, K. Balasubramanian, *J. Chem. Phys.* **1992**, *96*, 8345.

14 Z. Y. Lu, C. Z. Wang, K. M. Ho, *Phys. Rev. B* **2001**, *61*, 2329.

15 A. Hoareau, P. Melinon, B. Cabaud, D. Rayne, B. Tribollet, M. Broyer, *Chem. Phys. Lett.* **1988**, *143*, 602.

16 J. Ho, M. Polak, W. C. Lineberger, *J. Chem. Phys.* **1992**, *96*, 144.

17 See, for example: C. Xu, L. Manceron, J. P. Perchard, *J. Chem. Soc., Faraday Trans.* **1993**, *89*, 1291; V. E. Bondybey, A. M. Smith, J. Agreiter, *Chem. Rev.* **1996**, *96*, 2113; S. Fedrigo, T. L. Haslett, M. Moskovits, *J. Am. Chem. Soc.* **1996**, *118*, 5083; L. Khriachtchev, M. Pettersson, N. Runeberg, J. Lundell, M. Rasanen, *Nature* **2000**, *406*, 874; H. J. Himmel, L. Manceron, A. J. Downs, P. Pullumbi, *J. Am. Chem. Soc.* **2002**, *124*, 4448; J. Li, B. E. Bursten, B. Liang, L. Andrews, *Science* **2002**, *295*, 2242; L. Andrews, X. Wang, *Science* **2003**, *299*, 2049.

18 M. F. Zhou, G. V. Chertihin, L. Andrews, *J. Chem. Phys.* **1998**, *109*, 10893; M. F. Zhou, L. Andrews, *J. Chem. Phys.* **1999**, *110*, 10370.

19 B. Tremblay, G. Gutsev, L. Manceron, L. Andrews, *J. Phys. Chem. A* **2002**, *106*, 10525.

20 B. Tremblay, L. Manceron, G. Gutsev, L. Andrews, H. Partridge, III, *J. Chem. Phys.* **2002**, *117*, 8479.

21 M. F. Zhou, Z. X. Wang, P. von Ragué Schleyer, Q. Xu, *ChemPhysChem.* **2003**, *4*, 763; M. F. Zhou, N. Tsumori, L. Andrews, Q. Xu, *J. Phys. Chem. A* **2003**, *107*, 2458; M. F. Zhou, N. Tsumori, Z. H. Li, K. N. Fan, L. Andrews, Q. Xu, *J. Am. Chem. Soc.* **2002**, *124*, 12936.

22 L. Jiang, Q. Xu, *J. Am. Chem. Soc.* **2005**, *127*, 42.

23 a) M. F. Zhou, L. Jiang, Q. Xu, *J. Chem. Phys.* **2004**, *121*, 10474. b) L. Jiang, Q. Xu, *J. Chem. Phys.* **2005**, *122*, 034505. c) M. F. Zhou, L. Jiang, Q. Xu, *J. Phys. Chem. A* **2005**, *109*, 3325. d) B. Y. Liang, L. Andrews, *J. Phys. Chem. A* **2000**, *104*, 9156. e) L. Jiang, Q. Xu, *J. Phys. Chem. A* **2005**, *109*, 1026.

24 G. L. Gutsev, C. W. Bauschlicher, Jr., L. Andrews, *J. Chem. Phys.* **2003**, *119*, 3681.

25 Z. X. Cao, Y. J. Wang, J. Zhu, W. Wu, Q. E. Zhang, *J. Phys. Chem. B* **2002**, *106*, 9649.

26 I. S. Ignatyev, H. F. Schaefer, III, R. B. King, S. T. Brown, *J. Am. Chem. Soc.* **2000**, *122*, 1989.

27 M. F. Zhou, L. Andrews, C. W. Bauschlicher, Jr., *Chem. Rev.* **2001**, *101*, 1931.

28 H. J. Himmel, A. J. Downs, T. M. Greene, *Chem. Rev.* **2002**, *102*, 4191.

29 a) A. Bos, *J. Chem. Soc., Chem. Commun.* **1972**, 26. b) L. N. Zhang, J. Dong, M. F. Zhou, *J. Chem. Phys.* **2000**, *113*, 8700.

30 A. Feltrin, S. N. Cesaro, F. Ramondo, *Vib. Spectrosc.* **1996**, *10*, 139.

31 R. R. Lembke, R. F. Ferrante, W. Weltner, Jr., *J. Am. Chem. Soc.* **1977**, *99*, 416; A. D. Walters, W. Winnewisser, K. Lattner, B. P. Winnewisser, *J. Mol. Spectrosc.* **1991**, *149*, 542.

32 L. N. Zhang, J. Dong, M. F. Zhou, Q. Z. Qin, *J. Chem. Phys.* **2000**, *113*, 10169; L. N. Zhang, J. Dong, M. F. Zhou, *Chem. Phys. Lett.* **2001**, *334*, 335; Q. Y. Kong, M. H. Chen, J. Dong, Z. H. Li, K. N. Fan, M. F. Zhou, *J. Phys. Chem. A* **2002**, *106*, 11709; L. Miao, L. M. Shao, W. N. Wang, K. N. Fan, M. F. Zhou, *J. Chem. Phys.* **2002**, *116*, 5643.

33 T. R. Burkholder, L. Andrews, *J. Chem. Phys.* **1991**, *95*, 8697.

34 M. J. Frisch, G. W. Trucks, H. B. Schlegel, G. E. Scuseria, M. A. Robb, J. R. Cheeseman, J. A. Montgomery, Jr., T. Vreven, K. N. Kudin, J. C. Burant, J. M. Millam, S. S. Iyengar, J. Tomasi, V. Barone, B. Mennucci, M. Cossi, G. Scalmani, N. Rega, G. A. Petersson, H. Nakatsuji, M. Hada, M. Ehara, K. Toyota, R. Fukuda, J. Hasegawa, M. Ishida, T. Nakajima, Y. Honda, O. Kitao, H. Nakai, M. Klene, X. Li, J. E. Knox, H. P. Hratchian, J. B. Cross, C. Adamo, J. Jaramillo, R. Gomperts, R. E. Stratmann, O. Yazyev, A. J. Austin, R. Cammi, C. Pomelli, J. W. Ochterski, P. Y. Ayala, K. Morokuma, G. A. Voth, P. Salvador, J. J. Dannenberg, V. G. Zakrzewski, S. Dapprich, A. D. Daniels, M. C. Strain, O. Farkas, D. K. Malick, A. D. Rabuck, K. Raghavachari, J. B. Foresman, J. V. Ortiz, Q. Cui, A. G. Baboul, S. Clifford, J. Cioslowski, B. B. Stefanov, G. Liu, A. Liashenko, P. Piskorz, I. Komaromi, R. L. Martin, D. J. Fox, T. Keith, M. A. Al-Laham, C. Y. Peng, A. Nanayakkara, M. Challacombe, P. M. W. Gill, B. Johnson, W. Chen, M. W. Wong, C. Gonzalez, J. A. Pople, *Gaussian 03, Revision B.04*, Gaussian, Inc., Pittsburgh, PA, **2003**.

35 A. D. Becke, *J. Chem. Phys.* **1993**, *98*, 5648.

36 C. Lee, E. Yang, R. G. Parr, *Phys. Rev. B* **1988**, *37*, 785.

37 A. D. McLean, G. S. Chandler, *J. Chem. Phys.* **1980**, *72*, 5639; R. Krishnan, J. S. Binkley, R. Seeger, J. A. Pople, *J. Chem. Phys.* **1980**, *72*, 650.

38 P. J. Hay, W. R. Wadt, *J. Chem. Phys.* **1985**, *82*, 299.

39 J. H. Darling, J. S. Ogden, *J. Chem. Soc., Dalton Trans.* **1972**, 2496.